Monthly Notices of the ROYAL ASTRONOMICAL SOCIETY

MNRAS **528,** 2377–2390 (2024) https://doi.org/10.1093/mnras/stae143
Advance Access publication 2024 January 13

Constraints on cosmologically coupled black holes from gravitational wave observations and minimal formation mass

Luca Amendola,[1] Davi C. Rodrigues [1,2,3★] Sumit Kumar[4,5] and Miguel Quartin [3,6,7]

[1]*Institut für Theoretische Physik, Universität Heidelberg, Philosophenweg 16, D-69120 Heidelberg, Germany*
[2]*Departamento de Física & Cosmo-Ufes, Universidade Federal do Espírito Santo, 29075-910 Vitória - ES, Brazil*
[3]*PPGCosmo, Universidade Federal do Espírito Santo, 29075-910 Vitória - ES, Brazil*
[4]*Max-Planck-Institut für Gravitationsphysik (Albert-Einstein-Institut), D-30167 Hannover, Germany*
[5]*Leibniz Universität Hannover, D-30167 Hannover, Germany*
[6]*Instituto de Física, Universidade Federal do Rio de Janeiro, 21941-972 Rio de Janeiro, RJ, Brazil*
[7]*Observatório do Valongo, Universidade Federal do Rio de Janeiro, 20080-090 Rio de Janeiro, RJ, Brazil*

Accepted 2024 January 11. Received 2023 December 23; in original form 2023 August 1

ABSTRACT

We test the possibility that the black holes (BHs) detected by LIGO-Virgo-KAGRA (LVK) may be cosmologically coupled and grow in mass proportionally to the cosmological scale factor to some power k, which may also act as the dark energy source if $k \approx 3$. This approach was proposed as an extension of Kerr BHs embedded in cosmological backgrounds and possibly without singularities or horizons. In our analysis, we develop and apply two methods to test these cosmologically coupled BHs (CCBHs) either with or without connection to dark energy. We consider different scenarios for the time between the binary BH formation and its merger, and we find that the standard log-uniform distribution yields weaker constraints than the CCBH-corrected case. Assuming that the minimum mass of a BH with stellar progenitor is $2\,M_\odot$, we estimate the probability that at least one BH among the observed ones had an initial mass below this threshold. We obtain these probabilities either directly from the observed data or by assuming the LVK power-law-plus-peak mass distribution. In the latter case, we find at 2σ level, that $k < 2.1$ for the standard log-uniform distribution, or $k < 1.1$ for the CCBH-corrected distribution. Slightly weaker bounds are obtained in the direct method. Considering the uncertainties on the nature of CCBHs, we also find that the required minimum CCBH mass value to eliminate the tensions for $k = 3$ should be lower than $0.5\,M_\odot$ (again at 2σ). Finally, we show that future observations have the potential to decisively confirm these bounds.

Key words: black hole physics – gravitational waves – dark energy.

1 INTRODUCTION

Recently, a new intriguing hypothesis about the origin of the cosmic acceleration has been put forward by Croker & Weiner (2019); Croker, Runburg & Farrah (2020b), with further developments by Farrah et al. (2023b). According to this scenario, black holes (BHs) grow in mass due to a form of cosmological coupling unrelated to local accretion. If this growth is fast enough, it could compensate the decrease in number density due to the cosmic expansion, and generate a form of effective cosmological constant. These BHs deviate from the standard Kerr solution.[1] There is expectation that these solutions can be found within general relativity (GR) and that they could be singularity free (see also Dymnikova & Galaktionov 2016). These non-standard BH solutions are asymptotically Friedmann–Roberton–Walker, rather than Minkowski (Faraoni & Jacques 2007; Croker & Weiner 2019; Croker, Nishimura & Farrah 2020a; Croker, Runburg & Farrah 2020b). They could provide an average pressure that would constitute the entire amount of dark energy needed to explain the cosmic acceleration if the BHs have the necessary abundance. Farrah et al. (2023b) argue that this may be the case. In a companion paper, Farrah et al. (2023a) have found strong indication in favour of just such a cosmological growth of supermassive BHs in elliptical galaxies. This growth seems very difficult to explain in terms of the standard local growth channels of accretion. From different considerations, Gao & Li (2023); Cadoni et al. (2023a, b) provide further support for cosmologically coupled black holes.

This new BH solution is at the moment a conjecture, and in fact, criticisms on the above framework within GR have appeared. For instance, Avelino (2023) considers the use of gravastars as CCBHs, criticizes the mechanism for generating cosmological pressure assuming that the Birkhoff theorem can be applied and, additionally, points out that, if CCBH momentum is conserved, SMBHs could not be at rest with respect to their host galaxy. Parnovsky (2023) criticizes both the uncertainty in the estimation of SMBH data and the possibility of BHs to provide a negative pressure. Mistele

★ E-mail: davi.rodrigues@ufes.br

[1]Since astrophysical BHs are expected to have angular momentum, Kerr is a better description than Schwarzschild. Kerr BHs are asymptotically Minkowski and have a singularity 'dressed' by a horizon. Kerr-de Sitter solutions are also known (for a review see Akcay & Matzner 2011).

(2023) points out an inconsistency between the averaging process proposed by Croker & Weiner (2019) and the action principle; thus, this work also puts into question the proposed mechanism that generates the cosmological pressure. Wang & Wang (2023) argue that a cosmological coupling cannot exist within general relativity inside gravitationally bound systems. Here, we take an agnostic view and show how this may be at tension with GW data, independently of the detailed microphysics that may lead to the CCBH realization.

This paper is devoted to testing the cosmologically coupled BHs (CCBH) by looking at the current and future data sets from LIGO-Virgo-KAGRA (LVK). The current understanding is that the gravitational waves (GW) detected by LVK come from the merging of BHs with stellar progenitors. If the CCBH hypothesis is correct, they must have grown to the observed mass from an initially lower mass. However, BHs with a stellar progenitor cannot be formed with arbitrarily low masses. Observationally, there is evidence of a paucity of BH masses between 2–5 $M_\odot$ (Özel et al. 2010; de Sá et al. 2022; Abbott et al. 2023a), while there is no conclusive evidence for a BH with mass about or below 2 $M_\odot$ (see also Abbott et al. 2022). Our main results are based on the conservative mass threshold $m_{\rm th} = 2.0\,M_\odot$ as the minimum BH formation mass. However, we also consider changes in different values for this threshold. The higher (lower) is this threshold, the stronger (weaker) are our constraints. If in the future a stellar BH is detected with mass below 2 $M_\odot$, this will clearly imply that $m_{\rm th}$ has to be smaller than what is detected, weaking our constraints. In particular, the constraints would vanish for very low thresholds of $\lesssim 0.5\,M_\odot$. In Appendix A, we present further discussions on this.

In this paper, we use two complementary approaches, explore ways to alleviate the tensions[2] we find, and briefly discuss future prospects. We conclude that the CCBH as proposed by Farrah et al. (2023b) is in strong tension with what we know about stellar progenitor BHs, but there still is an open parameter space, where it can survive the present test. In particular, we find no relevant tension for the CCBH case studied by Croker et al. (2021). The forthcoming new GW data sets will soon shed further light on the CCBH conjecture.

The codes we used for this work are available at https://github.com/itpamendola/CCBH-direct and https://github.com/davi-rodrigues/CCBH-Numerics.

2 COSMOLOGICALLY COUPLED BLACK HOLES

Farrah et al. (2023a) considered three samples of red-sequence elliptical galaxies at different redshifts and found that the growth of supermassive BHs is significantly larger than the growth of stellar mass, being a factor of 20 from $z \sim 2$ to 0. This growth is too large to be compatible with the expected accretion rate (Farrah et al. 2023a). This suggests a different growth mechanism such that $m_{\rm BH} \propto m_*(1+z)^{-3.5\pm1.4}$, at 90 per cent confidence level, where m_* is the stellar mass of the galaxy and $m_{\rm BH}$ the supermassive BH mass of the same galaxy.

A possible explanation for the above physics comes from the proposal of cosmologically coupled BHs (CCBHs) (Faraoni & Jacques 2007; Croker & Weiner 2019; Croker et al. 2021). In this case, BHs would grow following the parametrization (Croker et al. 2021)

$$m(a) = m(a_i)\left(\frac{a}{a_i}\right)^k, \tag{1}$$

where $k \geq 0$ is a constant, a_i is the cosmological scale factor at the time of the BH formation and $m(a_i)$ is its mass at that time.

Farrah et al. (2023b) explore the viability of $k \approx 3$, which would both explain the supermassive BHs growth and provide a source of dark energy capable of generating the observed Ω_Λ value. The latter requires further assumptions, in particular a proper star formation rate, that all the remnants with mass >2.7 $M_\odot$ are BHs, and that all the BHs follow the above mass parametrization. Beside the theoretical issues commented in Section 1, Lei et al. (2024) used JWST data and found a conflict with Farrah et al. (2023a) parametrization at redshifts $z \sim 4.5$–7. These high redshift results are mostly independent of our analysis: the constraints we find come from lower redshifts, as will be shown when constraining the maximum redshift of binary BH formation ($z_{\rm max}$).

If all BHs are cosmologically coupled with $k = 3$, Rodriguez (2023) pointed out that this would be in contradiction with globular cluster NGC 3201 data, since it would imply that one of the BHs would have a mass below 2.2 $M_\odot$. A similar test on two *Gaia* DR3 stellar-BH systems with reliable age estimation has been carried out by Andrae & El-Badry (2023), resulting in the 2σ upper limit $k \leq 3.2$ assuming the same 2.2 $M_\odot$ limit and fixing the background to ΛCDM. In Appendix A, we detail further aspects of the BH minimum mass in the context of CCBH.

Ghodla et al. (2023) found that the rate of mergers and their typical masses in a CCBH scenario would be hardly compatible with LVK observations; they also point out that CCBHs should exhibit lower spins due to their increase in mass. They have also derived a modified delay time for CCBHs that we consider in Section 6. This modified delay time makes CCBHs more incompatible with current data, as we develop here.

Our purpose here is to test if the BHs detected from their coalescence waves could be cosmologically coupled. Before the results from Farrah et al. (2023b), Croker et al. (2021) (see also Croker, Nishimura & Farrah 2020a) developed simulations of merging BHs and considered the impact of the cosmological coupling on the LVK detected BHs, showing that $k = 0.5$ would be preferred over the standard $k = 0$, at least for certain isolated-binary-evolution model. We use here the most recent data from LVK, together with more recent delay time expectations. A crucial difference between this work and the works of Croker et al. (2021); Ghodla et al. (2023) on CCBH and LVK data is that they started from a given BBH formation mass, assumed to be realistic, and consider if they could mimic LVK data from that initial mass distribution. Here we aim to estimate what is the probability that at least one of the observed BHs via LVK would be formed with a mass below a given threshold mass (thus in part similar to Rodriguez 2023). A key quantity for modelling the CCBH effects on LVK data is the delay time $t_{\rm d}$ (i.e. the interval between BBH formation and merger), which is detailed in Section 3.

Within the general class of CCBHs, we distinguish two cases. If BHs have dark energy implications and constitute its only source, as proposed in (Croker, Runburg & Farrah 2020b; Farrah et al. 2023b), then the constant k, which parametrizes the energy density of BHs as a function of $a(t)$, has a direct connection with the dark energy equation of state parameter w, with

$$k \equiv -3w. \tag{2}$$

We call this scenario dark energy BHs, DEBH.

If CCBHs masses increase following equation (1), but if they do not constitute a dark energy source, we call these growing BHs (GBHs). For instance, Croker et al. (2021) considered BHs with this property with $k = 0.5$. This picture can be realized if the CCBHs

[2]We use the word 'tension' for rejections at a level higher than 2σ.

contribution to the total cosmological energy density is negligible, or if GBHs are receiving energy with another field, say an additional scalar field. In the GBH scenario, dark energy is fully sourced by a cosmological constant and there is no deviation from ΛCDM background cosmology.

The two models, DEBH and GBH, have identical background cosmological evolution for $k = 3$ but diverge otherwise. We consider both in the following.

3 DELAY TIME AND THE MASS CORRECTING FACTOR

The merging of binary black holes (BBH) systems detected by LVK is commonly considered to be the end of a pair of BHs that orbited together from several Myrs to several giga-years before the merger (Abbott et al. 2021a). These BHs masses are consistent with them being remnants of star progenitors, and this constitutes the standard interpretation (e.g. Belczynski et al. 2016; Mapelli 2020; Chen, Lu & Zhao 2022; van Son et al. 2022; Abbott et al. 2023a).

The relevant time during which the CCBH effect (1) is active extends between the BHs formation and their merger. We call this time the BBH delay time and denote it by $t_{\rm d}$. We note that another delay-time definition, as the time between the stellar pair formation and the BBH merger, is also used in the literature. However, they typically differ by a few Myr (van Son et al. 2022), hence both definitions are essentially the same.

For the GBH scenario, we consider any value of k in the range $0 \leq k \leq 3$ (Croker et al. 2021), where $k = 0$ corresponds to the standard case (uncoupled Kerr BHs). Apart from the $k = 3$ case, other values of particular interest that have been discussed in the literature are $k = 0.5$ (Croker et al. 2021) and 1 (Cadoni et al. 2023b).

For the DEBH case, changing the k value changes cosmology. For clarity, this case will be parametrized with a constant w, instead of k. We mainly consider $-0.6 \leq w \leq -1$. We do not consider more negative w values since they can only strengthen our constraints. The DEBH scenario has no limit that leads simultaneously to standard BHs and standard background cosmology.

Abbott et al. (2021a, 2023a) state that the distribution of delay times can be approximated by a log-uniform distribution (i.e. $p(t_{\rm d}) \propto 1/t_{\rm d}$) with $0.05 < t_{\rm d}({\rm Gyrs}) < 13.5$ for BBHs. It is also pointed out that the formation of the first BBHs is restricted to $z < 10$. This picture is in good agreement with simulations and observational constraints (e.g. Belczynski et al. 2016; Fishbach & Kalogera 2021; van Son et al. 2022).

CCBHs, on the other hand, grow with time and therefore their delay times will also change: since larger BH masses dissipate energy faster through GW emission, the delay time of CCBHs should be smaller than for ordinary BHs for the same initial mass and orbit (Croker, Runburg & Farrah 2020b; Ghodla et al. 2023; Farrah et al. 2023b). This does not imply that the delay time distribution of the *detected* BBH mergers will favour shorter times. In particular, as commented by Ghodla et al. (2023); Farrah et al. (2023b), BBHs that would not merge before $z = 0$ in the standard picture may merge if CCBH is true. We will explore in more detail the possible CCBHs changes to the $t_{\rm d}$ distribution in Section 6 and Appendix B. Of particular relevance, there it is shown that the CCBH corrections to the delay-time distribution favour larger delay times than the log-uniform distribution. Therefore, studying the log-uniform case is useful also because it provides conservative bounds.

Due to such unknowns, we use a log-uniform distribution for $t_{\rm d}$ varying three parameters that have a direct impact on the $t_{\rm d}$ values ($t_{\rm min}$, $t_{\rm max}$, and $z_{\rm max}$, as detailed below). Moreover in Appendix C, we explore the possibility of a steeper PDF for the $t_{\rm d}$ distribution (i.e. smaller delay times on average), which reduces the tensions we find in the main analysis.

We adopt then here the log-uniform $t_{\rm d}$ distribution,

$$\log t_{\rm d} \sim U(\log t_{\rm min}, \log t_x), \tag{3}$$

where t_x is the minimum between the maximum delay time $t_{\rm max}$ and the time difference between the merger redshift ($z_{\rm m}$) and the maximum redshift with BBH formation ($z_{\rm max}$). As *reference values*, we consider

$$\begin{aligned} t_{\rm min} &= 0.05\,{\rm Gyr}, \\ t_{\rm max} &= 13.0\,{\rm Gyr}, \\ z_{\rm max} &= 10, \\ w &= -1, \\ k &= 3. \end{aligned} \tag{4}$$

Besides these reference values, we also explore other combinations. We anticipate that the CCBH tension that we find here either increases or stays constant if $t_{\rm max}$, $z_{\rm max}$, or $t_{\rm min}$ are increased. For the cosmological model, we assume $\Omega_{\rm m} = 0.32$ and $H_0 = 70\,{\rm km\,s^{-1}\,Mpc^{-1}}$.

Fishbach & Kalogera (2021) studied a possible correlation between $t_{\rm d}$ and m_1 considering observational data. It was found a marginal preference for smaller masses values to have larger $t_{\rm d}$. We do not consider such a correlation here, but if future analyses confirm this mass delay-time correlation, it will result in stronger bounds on the CCBH model from GW data. In any case, the true delay-time distribution and its dependence on the mass are still uncertain (e.g. van Son et al. 2022).

Let us now consider a BH that is formed at z_i and merges after a delay time $t_{\rm d}$ at $z_{\rm m}$. Then

$$t_{\rm d} = \int_{z_i}^{z_{\rm m}} \frac{{\rm d}z}{(1+z)H(z)}. \tag{5}$$

This can be inverted for a given w using

$$H^2 = H_0^2\left[\Omega_{\rm m}(1+z)^3 + (1-\Omega_{\rm m})(1+z)^{3+3w}\right], \tag{6}$$

leading to

$$z_i = z_i(z_{\rm m}, t_{\rm d}). \tag{7}$$

Then the initial mass mi of BHs will be a function of $z_{\rm m}$, $t_{\rm d}$, k, and proportional to the mass $m_{\rm m}$ at merging time,

$$m_i = m_{\rm m}\left(\frac{1+z_{\rm m}}{1+z_i(z_{\rm m}, t_{\rm d})}\right)^k. \tag{8}$$

From a given set of observed BHs masses and a $t_{\rm d}$ distribution (3), we aim to find the probability that none of the observed BHs was formed with mass below the mass threshold $m_{\rm th}$ (i.e. $M_i < m_{\rm th}$). If this probability is close to 1, then there is no tension between observations and the CCBH model. Otherwise, there is tension between the observational data, the model and the given assumptions. We will show that the latter is the case. Alternatively, one should invoke significant changes in some of the basic assumptions, e.g. a lower threshold for BH formation, shorter delay times, a late BH formation, or a different growth scheme.

We estimate this probability in two complementary ways. In the first one, we use directly the current data set and find the joint probability that at least one BH was born with a mass below threshold under the CCBH hypothesis. Since we do not correct the observed

Table 1. Selected confident GW events from GWTC-3 catalogue (Abbott et al. 2023b) that are classified in (Abbott et al. 2023a) as BBH or NSBH systems (we require $p_{\rm astro} > 0.5$ and $\mathrm{FAR}_{\rm min} < 1\,\mathrm{yr}^{-1}$), for a total of 72 events. The columns show the event name, the merging redshift and the primary and secondary masses. The full table is provided electronically.

Event	$z_{\rm m}$	m_1 ($\mathrm{M}_\odot$)	m_2 ($\mathrm{M}_\odot$)
GW150914	$0.090^{+0.030}_{-0.030}$	$35.6^{+5.}_{-3.1}$	$30.6^{+3.0}_{-4.}$
GW151012	$0.21^{+0.09}_{-0.09}$	$23.^{+15.}_{-6.}$	$14.^{+4.}_{-5.}$
GW151226	$0.09^{+0.04}_{-0.04}$	$13.7^{+9.}_{-3.2}$	$7.7^{+2.2}_{-2.5}$
GW170104	$0.20^{+0.08}_{-0.08}$	$31.^{+7.}_{-6.}$	$20.^{+5.}_{-5.}$
GW170608	$0.070^{+0.020}_{-0.020}$	$11.0^{+6.}_{-1.7}$	$7.6^{+1.4}_{-2.2}$
...	...	...	...

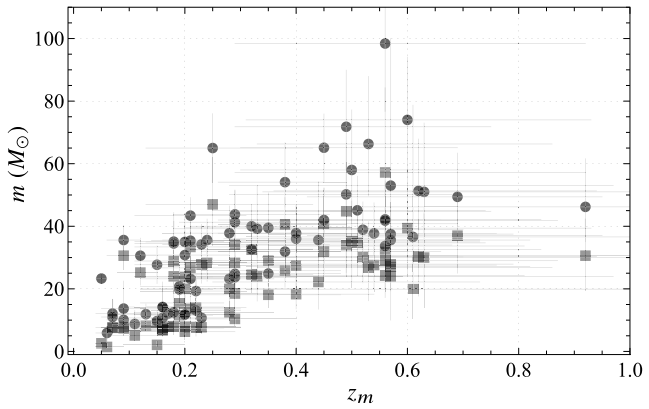

Figure 1. The distribution of m_1 (discs) and m_2 (squares) as a function of the merging redshift ($z_{\rm m}$). Data from Table 1.

distribution for the selection effects, we implicitly discard low-mass BHs from the estimation, and therefore we end up with more conservative, but possibly more robust, estimates. We call this the *direct method*. In the second method, we derive the expected initial mass distribution of BHs taking into account the selection bias of the detectors through the power-law-plus-peak (PLPP) profile (Abbott et al. 2021b, 2023a). This method leads to stronger constraints. We denote this as the *PLPP method*.

The GWTC-3 data we use are shown in Table 1 and in Fig. 1. These data come from confident BBH and NSBH events (Abbott et al. 2023b, 2023a) that satisfy $p_{\rm astro} > 0.5$ and $\mathrm{FAR}_{\rm min} < 1\,\mathrm{yr}^{-1}$. In our analysis, we use separately either the primary m_1 masses or the secondary m_2 ones. Therefore, each selected mass corresponds to an independent history of a compact binary evolution and merger. Considering all the m_1 and m_2 in a single analysis would be incorrect since binary BHs have the same $t_{\rm d}$ and would therefore not be independent. Although we consider here results with either primary or secondary masses, emphasis is given on the results for m_1 masses, since these produce more robust and more conservative constraints. For the direct method, this choice automatically removes BHs that are outliers with particularly low mass and have a large impact on the statistics used. For the PLPP method, the m_1 data is more robust since its distribution depends on one less parameter, with non-negligible uncertainty, than the m_2 distribution. In principle, one could consider m_2 masses for all the BBH cases, and change to m_1 masses for the NSBH systems, but the impact on the results is small since there are only one or two NSBH systems in our selected sample.

The selected sample, Table 1, has only two systems classified as NSBH by LVK, namely: GW200105_162426 and GW190917_114630. This classification depends on the adopted minimum mass for BHs, and Abbott et al. (2023a) consider $2.5\,\mathrm{M}_\odot$. When considering that the minimum mass is $2\,\mathrm{M}_\odot$, there remains a single NSBH, GW200115_042309. Excluding all events with secondary mass less than $5\,\mathrm{M}_\odot$ as potential NS or outliers, we are left with 69 m_2 data points.

4 DIRECT CONSTRAINTS FROM THE OBSERVED EVENTS

Here, we discuss the direct method. The formation redshift that a BH of merging mass $m_{\rm m}$ observed at $z_{\rm m}$ should have to initially form with a given threshold mass $m_{\rm th}$ is given by equation (8) as

$$z_{\rm th} = (1 + z_m)\left(\frac{m_{\rm m}}{m_{\rm th}}\right)^{1/k} - 1, \tag{9}$$

and the corresponding delay time is

$$t_{\rm th} = t_{\rm d}(z_{\rm m}, z_{\rm th}) = t_{\rm d}(z_{\rm m}, m_{\rm m}, m_{\rm th}). \tag{10}$$

If the delay time is larger than $t_{\rm th}$, the BH would have formed with a mass below the threshold. If $t_{\rm th}$ plus the merger age $t(z_{\rm m})$ is larger than the cut-off $t_{\rm max}$, we take $t_{\rm th} = t_{\rm max} - t(z_m)$. Analogously, if $z_{\rm th}$ is larger than, say, $z_{\rm max} = 10$, we should cut it at $z_{\rm max}$ to prevent formation at an unrealistically early epoch. Now, given a normalized delay-time distribution $\Psi(t_{\rm d})$, the probability that a BH has formation mass above $m_{\rm th}$ is

$$p_i(z_{\rm m}, m_{\rm m}, m_{\rm th}) = \int_0^{t_{\rm th}} \Psi(t_{\rm d})\,\mathrm{d}t_{\rm d}. \tag{11}$$

The combined probability of having N BHs within the acceptable formation mass range $> m_{\rm th}$ is

$$P(m_1 > m_{\rm th}) = \prod_i^N p_i \tag{12}$$

and therefore the probability of at least one below-threshold BH is $1 - P$. In order to reject the CCBH hypothesis at given k, we should find a small P for the currently observed BHs. In other words, the p-value for rejecting the CCBH hypothesis is $p = P(m_1 > m_{\rm th})$.

Since GW observations pick preferentially high-mass BHs, the constraints we derive are on the conservative side.

We consider both the DEBH case, in which the BH growth is linked to the dark energy so that $k = -3w$, and the alternative GBH scenario in which the BH growth does not influence the cosmological expansion. For simplicity, in this second case, we fix $w = -1$, i.e. the standard cosmological constant. In each case, there is then just one BH-cosmological parameter (in addition to the astrophysical ones, namely $t_{\rm min}$, $t_{\rm max}$, $z_{\rm max}$, $m_{\rm th}$): either k for the GBH case or w for the DEBH case.

We also notice that the merger redshifts $z_{\rm m}$ are obtained from the luminosity distance by assuming a ΛCDM evolution. However, in the DEBH scenario, the background is ΛCDM only for $w = -1$ so for any other value of w we should derive a new set of $z_{\rm m}$. This correction is however on average $\Delta z = 0.02$ for $w = -0.6$, and smaller for w closer to -1. This is negligible with respect to the current uncertainty in $z_{\rm m}$, so we neglect it.

We illustrate in the corner plot Fig. 2, the exclusion plots for various combinations of parameters for both scenarios, implicitly fixing all the other parameters to the reference case described above in equation (4). In this and in the subsequent corner plot, the reference

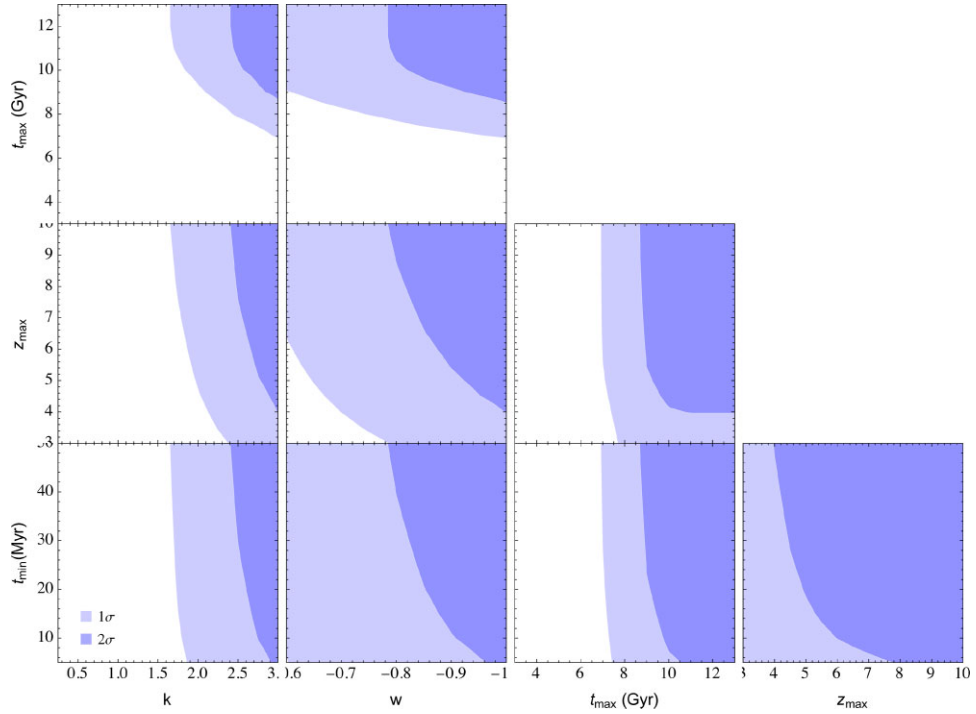

Figure 2. Direct method. Exclusion plots for the GBH and DEBH tensions. Here, we assume a minimum mass threshold $m_{th} = 2\,M_\odot$. The reference values are always in the upper right corner of each plot. The first and second column correspond respectively to the GBH and the DEBH cases. The two last columns show results that are common to both approaches.

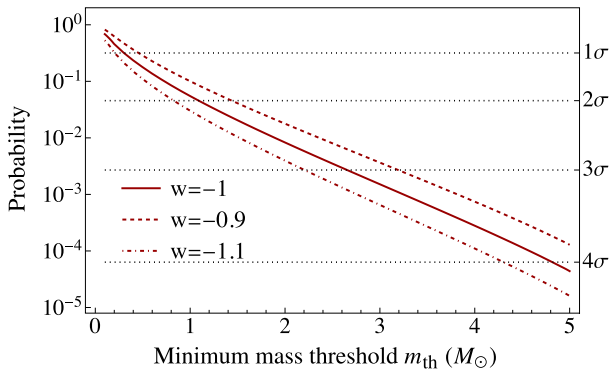

Figure 3. Direct method. Plot of $P(m_1 > m_{th})$ versus minimum BH mass in the DEBH scenario. The dotted horizontal lines mark the σ levels.

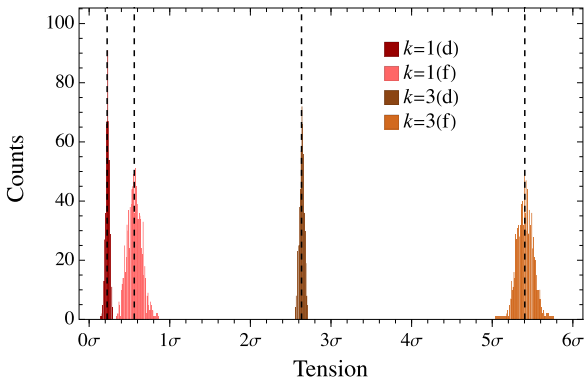

Figure 4. Direct method. Tensions assuming a fixed threshold $m_{th} = 2\,M_\odot$ and the reference t_d values (4) for current data (d) and for the forecasted 250 LVK O4 events (f) obtained as 1000 random realizations of the current GW data, for $k = 1$ and 3. The vertical black dashed lines show the median value of each distribution.

case (for which GBH and DEBH coincide) is always at the upper right corner; moving beyond this point increases the rejection level of the CCBH hypothesis.

The main result is that, for DEBH and in the reference case, the probability of having no BHs below threshold is 0.0083, corresponding to 2.64σ. Using instead the m_2 masses, and excluding as potential outliers (perhaps neutron stars), the two compact objects with masses in the range 2–5 $M_\odot$, we obtain, as expected, a higher rejection level of 3.05σ. Decreasing w into the phantom regime $w < -1$ makes the result stronger. For $w < -1.2$, using m_1 masses the rejection is at the 3σ level (again, fixing all the other parameters to reference). For the other parameters, the range for which the tension is reduced below the 2σ level are $t_{max} < 8.7$ Gyr and $z_{max} < 4$.

For $k \approx 3$, the dependence on the threshold mass is shown in Fig. 3. Using the references values, the tension is removed only if the minimum BH mass is lower than 1.1 $M_\odot$ for $k = 3$. Within the DEBH scenario, that is, considering changes of the dark energy equation of state induced by $k = -3w$, the minimum BH mass should be below 1.4 $M_\odot$ for $w = -0.9$, or below 0.9 $M_\odot$ for $w = -1.1$.

In Fig. 4, we show the distribution of probabilities for 1000 realizations of the current data randomly chosen. The mass and redshift distribution for each event has been obtained from the posteriors samples of the latest GWTC data release (Abbott et al. 2019, 2023b, 2024). We use source frame mass distribution for each event. This narrow distribution shows that sticking with the best fit z_m, m_m values is an acceptable approximation. For the forecast and $k = 3$, the rejection level goes beyond 5σ. On the other hand, for $k = 1$ even the forecasted data implies no relevant tension.

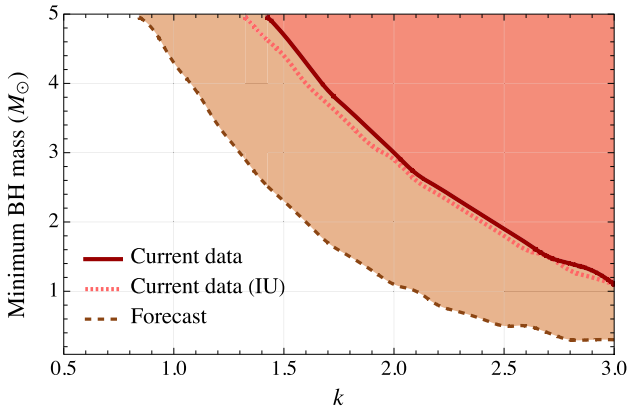

Figure 5. Direct method. Excluded 2σ regions for current data (72 events, red) and forecast (250 events, brown). The GBH model is used here. The solid red line uses the observed mass and redshift distributions of all 72 events. The dotted red line is the resulting 2σ exclusion line based on the 72 events central values, that is, ignoring uncertainties (IU). The forecast assumes no changes in the mass-redshift distribution and considers 250 events.

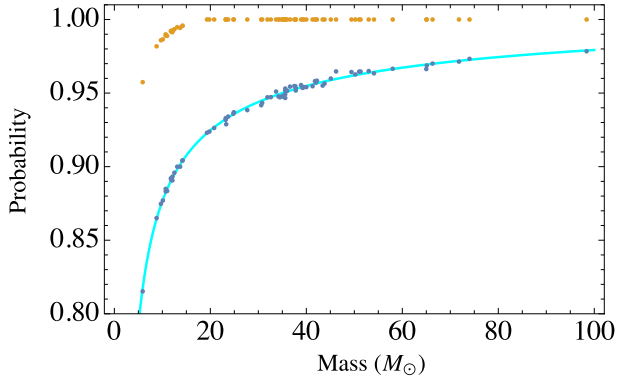

Figure 6. Direct method. Individual probabilities for each BH to be formed with a mass above the $2\,M_\odot$ threshold, as a function of its observed mass at merging. The cyan curve is the best fit given by equation (13) for the reference case $k = 3$. The small dispersion about the curve is due to differences in the observed redshift. The orange dots represent the probabilities for $k = 1$; they are, of course, much closer to unity.

In the same Fig. 4, we also estimate $P(m_1 > m_{\rm th})$ for a number of future events. After 4 months LVK O4 run has observed 44 significant BBH candidate events.[3] If we further limit ourselves to those with preliminary $\mathrm{FAR_{min}} < 1\,\mathrm{yr}^{-1}$ and preliminary BBH classification with over 90 per cent probability, 35 BBH candidates remain. Considering that O4 should last for 20 months, and that Virgo has not yet joined observations, one expects as a very conservative lower bound a total of $20/4 \times 35 = 175$ new BBH events (or 247 in total) by the end of O4. Therefore, we assumed 250 BBH events for our O4 forecasts in Fig. 4 and below.

Fig. 5 explores the two most relevant parameters for this analysis, k and minimum BH mass ($m_{\rm th}$), considering the observational distribution of the pair ($z_{\rm m}$, m_1) for each detected event. We use here the GBH picture, since the DEBH one changes significantly the cosmology if k is not close to 3. The main result is the red solid line that delimits the 2σ excluded region using the current LVK data. To find this curve, we proceed as follows: for each pair of values (k, $m_{\rm th}$) and a particular realization of the observational data distribution, we compute the probability that there is no BH with mass below $m_{\rm th}$. We repeat the previous evaluation for 300 realizations of the observational data distribution. A point in the 2σ curve corresponds to the 95 per cent quantile of the previous 300 realizations.

We stress the following results at 2σ level for the current and the forecast data: *i*) assuming $m_{\rm th} = 2\,M_\odot$ for the minimum BH mass: $k < 2.5$ (current) and 1.6 (forecast). *ii*) for $k = 3$, $m_{\rm th} < 1.1$ (current) and $0.3\,M_\odot$ (forecast). For $k = 1$, there are no constraints from the current data and the forecast yields a very weak $m_{\rm th}$ constraint. For $k = 0.5$, there are no constraints from this approach.

Finally, in Fig. 6, we plot the individual probabilities p_i as a function of the BH mass for the reference case. As expected, small BHs are more likely to originate from below-threshold masses. However, all values of p_i are relatively close to unity (larger than 0.8), implying that currently observed BH are more likely to be formed above the threshold than below it. It is the combined probability, rather than some peculiar outlier, that leads to the conclusion that at least one BH should have been formed below threshold.

[3] https://gracedb.ligo.org/superevents/public/O4/

We find that, apart from a small dispersion that depends on the merging redshift ($z_{\rm m}$), the probability $p(m)$ for a BH of observed mass m (in solar mass units) can be very well approximated in the reference case by the following function

$$p(m) = C \log(A - Bm^{-1/2}), \tag{13}$$

with $A = 26.72$, $B = 30.88$, $C = 0.3096$. The form of this function is suggested by the analytical integration of equations (5) and (11) for a pure CDM model and a $1/t_{\rm d}$ distribution; the coefficients are then obtained as a best fit to the actual p_i values.

5 CONSTRAINTS USING THE POWER-LAW-PLUS-PEAK DISTRIBUTION

5.1 General procedures

We now move to the PLPP method. The true population of merged BBHs is not well described by the detected BBHs since detection bias has an important role. In particular, it is known that it is easier to detect massive BBH systems than low-mass systems: many low-mass BBH mergers are expected to happen but are undetected.

A successful profile for the mass distribution of merged BBHs (i.e. after modelling and correcting the detection bias) is the power-law-plus-peak (PLPP) one, as proposed by Talbot & Thrane (2018) and analysed with current data (Abbott et al. 2021b, 2023a). Considering the m_1 mass distribution, the PLPP is a combination of a power law, described by $\beta(m_1)$, a Gaussian peak given by $G(m_1)$, and a smoothing function $S(m_1)$ that smooths the minimum mass probability transition. The PLPP depends on seven parameters to describe the m_1 distribution: the power α, the minimum and maximum masses ($m_{\rm min}$, $m_{\rm max}$), the Gaussian mean and standard deviation (μ, σ), the smoothing parameter $\delta_{\rm m}$, and the λ parameter that adjusts the relative importance of the peak and the Gaussian. The peak is interpreted as a consequence of pair-instability supernovae (Talbot & Thrane 2018). The smoothing function S is introduced since the most probable m_1 values are not expected to be at the minimum $m_{\rm min}$: expectations from X-ray binaries and simulations (Talbot & Thrane 2018) suggest a smoother transition. Explicitly, the

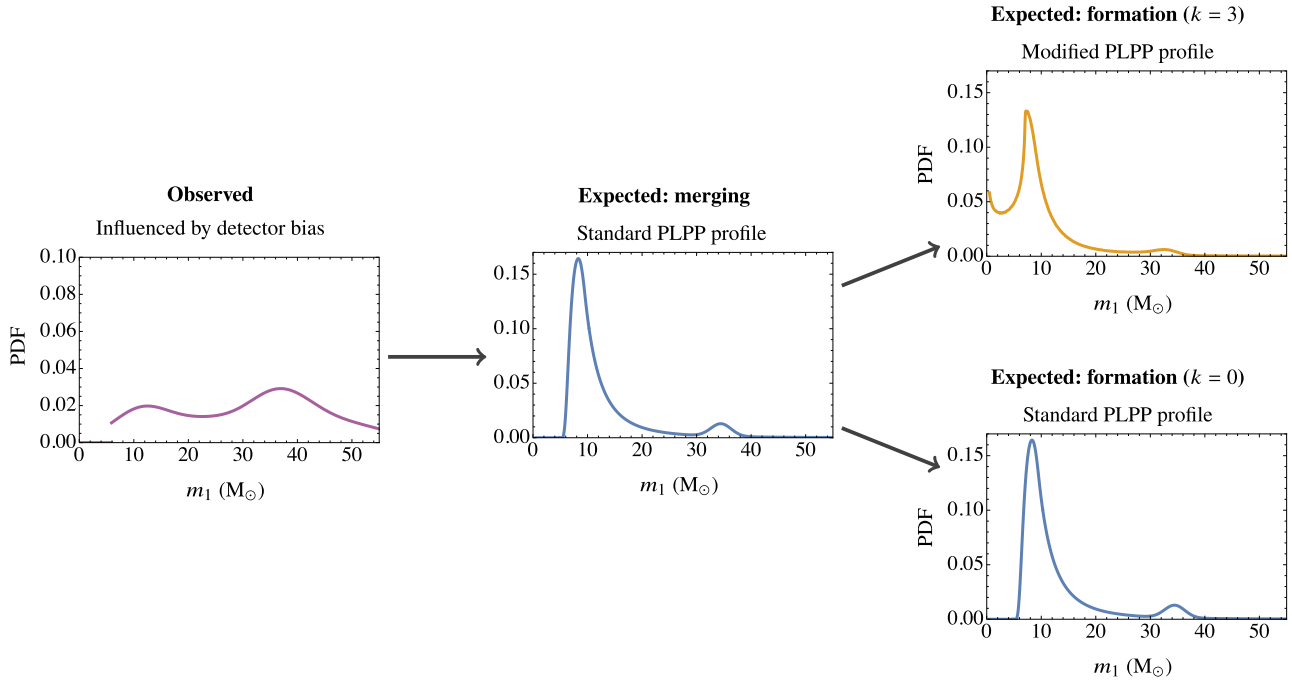

Figure 7. PLPP method. Illustration of the relation between three m_1 distribution contexts: the detected distribution, the expected distribution of all the m_1 masses from BBHs that merge (considering observational bias), and the expected m_1 distribution when it was formed. In the standard picture ($k = 0$, $w = -1$), the distributions for formation and merging are the same. For CCBH, between formation and merger, BHs increase their mass, hence the formation distribution will favour lower masses than the standard picture.

PDF reads,

$$\begin{aligned}
\pi(m_1) &\propto (1-\lambda)\beta(m_1)S(m_1) + \lambda G(m_1)S(m_1),\\
\beta(m_1) &= \frac{\alpha - 1}{m_{\rm min}^{1-\alpha} - m_{\rm max}^{1-\alpha}} m_1^{-\alpha},\\
G(m_1) &= \frac{1}{\sqrt{2\pi}\sigma}\exp\left(-\frac{(m_1-\mu)^2}{2\sigma^2}\right),\\
S(m_1) &= \begin{cases} \left[1+\exp\left(\frac{\delta_{\rm m}}{\delta m_1} - \frac{\delta_{\rm m}}{\delta m_1 - \delta_{\rm m}}\right)\right]^{-1}, & \delta m_1 < \delta_{\rm m}\\ 1, & \delta m_1 > \delta_{\rm m}, \end{cases}
\end{aligned} \tag{14}$$

where $\delta m_1 \equiv m_1 - m_{\rm min}$. It is also imposed that $\pi(m_1) = 0$ for $m_1 < m_{\rm min}$ or $m_1 > m_{\rm max}$. The PLPP parameter $m_{\rm min}$ states the minimum mass for both m_1 and m_2 masses. It should not be interpreted as stating the minimum mass of any BH; it is a fitted parameter that best describes the BBH merging population assuming that the PLPP profile holds. If this parameter is decreased, lower masses for the merging BBH population are possible; hence, in the CCBH context, even lower masses are necessary at formation time. Lowering $m_{\rm min}$ increases the constraints we find, while larger $m_{\rm min}$ values will decrease them. There is an analogous behaviour in the direct approach, in the sense that the lower the detected mass at merger time, the stronger will be our constraints.

The parameters are found from GW observational data and considering the detector bias, through a hierarchical Bayesian approach (Abbott et al. 2023a). The PLPP model represents the source frame mass distribution corrected for the selection effects. For the GWTC-3 data, the eight parameters that describe the m_1 and m_2 distributions are (LIGO Scientific Collaboration, Virgo Collaboration & KAGRA Collaboration 2023) (90 per cent credible intervals):

$$\begin{aligned}
\alpha &= 3.40^{+0.58}_{-0.49}, & \delta_{\rm m} &= 4.8^{+3.3}_{-3.2}\,{\rm M}_\odot,\\
m_{\rm min} &= 5.08^{+0.87}_{-1.5}\,{\rm M}_\odot, & m_{\rm max} &= 86.9^{+11.}_{-9.4}\,{\rm M}_\odot,\\
\mu &= 33.7^{+2.3}_{-3.8}\,{\rm M}_\odot, & \sigma &= 3.6^{+4.6}_{-2.1}\,{\rm M}_\odot,\\
\lambda &= 0.039^{+0.058}_{-0.026}, & \beta_{\rm q} &= 1.1^{+1.8}_{-1.3}.
\end{aligned} \tag{15}$$

The $\beta_{\rm q}$ parameter, only needed to describe the m_2 distribution, will be discussed later on. The central values above are the medians of the posteriors, while the uncertainties represent the 5 and 90 per cent quantiles of the posteriors. From (LIGO Scientific Collaboration, Virgo Collaboration & KAGRA Collaboration 2023), we also infer the maximum likelihood values, which read,

$$\begin{aligned}
&\alpha = 3.55, m_{\rm min} = 4.82\,{\rm M}_\odot, m_{\rm max} = 83.14\,{\rm M}_\odot,\\
&\delta_{\rm m} = 5.45\,{\rm M}_\odot, \mu = 34.47{\rm M}_\odot, \sigma = 1.87\,{\rm M}_\odot,\\
&\lambda = 0.019, \beta_{\rm q} = 0.76.
\end{aligned} \tag{16}$$

To test the CCBH hypothesis, we use the merging BBH distribution, as provided by PLPP, to find the expected BBH mass distribution by the formation time, as illustrated in Fig. 7. More precisely, let $M_{1,\,{\rm m}}$ be a random realization of the PLPP distribution, where the index m stands for merger time, and let F_{z_m} be a random realization of the mass factor correction of equation (8) at given $z_{\rm m}$. Then the m_1 distribution at BBH formation time is the distribution of the random variate $M_{1,\,i}$, with

$$M_{1,i} = F_{z_{\rm m}} M_{1,{\rm m}}. \tag{17}$$

Our results are found using at least 10^5 realizations of each random variable.

A *caveat* of the above procedure is that the mass factor distribution depends on $z_{\rm m}$, hence the m_1 distribution by formation time is $z_{\rm m}$ dependent. This dependence on $z_{\rm m}$ can be either considered by using

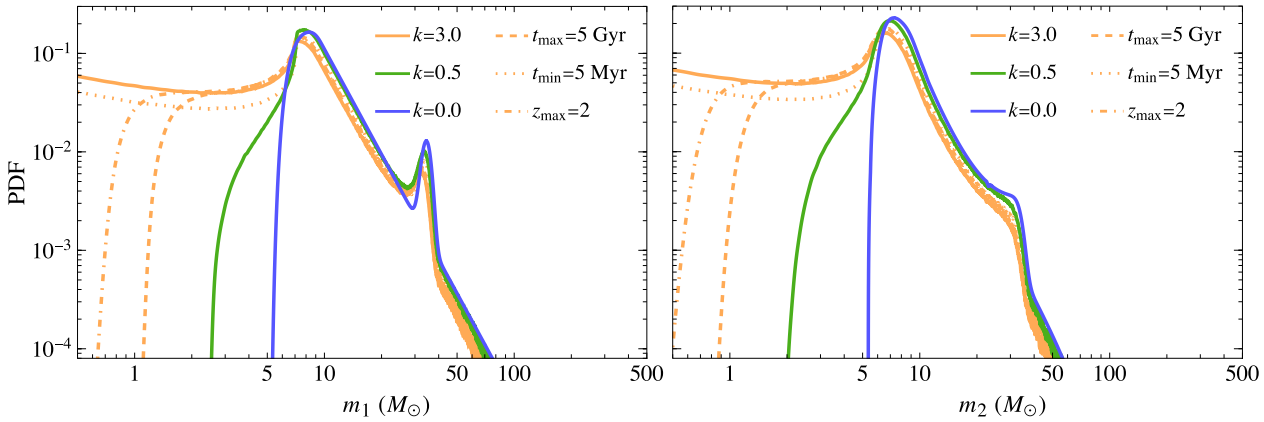

Figure 8. PLPP method. The m_1 (left plot) and m_2 (right plot) distributions at formation for different parameter values, assuming the PLPP distribution at merger (see Fig. 7, using PLPP parameters of equation (16)). In blue, we show the $k = 0$ case (no cosmological coupling). The green line shows the $k = 0.5$ case, within the GBH approach. The solid orange curve show the case $k = 3$ with the reference values equation (4); while the other three orange curves show variations with respect to the latter values: $t_{max} = 5$ Gyr (dashed), $t_{min} = 5$ Myr (dotted) and $z_{max} = 2$ (dot–dashed). The plots were generated with 10^7 simulated events.

the z_m values from observations or by using a mean z_m value as an approximation. The dependence on z_m is weak (see also Fig. 6), thus simply using an average z_m value is sufficient. The quality of the approximation can be directly verified by computing any probability at the minimum and maximum z_m values.

From the m_1 mass distribution at the BBH formation, one can compute what is the probability that one of the merged BBHs could have been formed with m_1 larger than a given mass threshold m_{th}, denoted by $p(m_{th}, z_m)$. For the various scenarios studied here, this probability for a single event with a mass larger than $2\,M_\odot$ is not far from, but clearly below, unity. Since the total number of merged BBHs is larger than the total number of confidently detected mergers, a minimum bound can be found by using the confidently detected BHs from gravitational waves (denoted by N), which we will use here. Hence, the probability of a given CCBH realization being compatible with existing data, similarly to equation (12), is

$$P(m_1 > m_{th}) = \prod_j^N p_j(m_{th}, z_{m,j}) \approx p^N(m_{th}, \overline{z_m}), \tag{18}$$

where $\overline{z_m}$ is an average over all the $z_{m,j}$ values. The above equation can be computed either using the redshift values of the observed merged BBH or by using the last approximation, which only depends on $\overline{z_m}$. The numerical differences are small, being negligible when stating the tension with σ units.

The above analysis applies for m_1 masses. Following Talbot & Thrane (2018), the m_2 distribution is given by the following conditional probability,

$$\pi(m_2|.m_{.1}) \propto \left(\frac{m_2}{m_1}\right)^{\beta_q} S(m_2)\Theta(m1 - m_2), \tag{19}$$

where β_q is the single PLPP parameter that only appears in the m_2 distribution, S is the smoothing function as defined in (14), and Θ is the Heaviside theta function. In order to find the PDF $\pi(m_2)$, we marginalize over m_1,

$$\pi(m_2) = \int_{m_{min}}^{m_{max}} \pi(m_2|.m_{.1})\pi(m_1)\,dm_1, \tag{20}$$

where $\pi(m_1)$ is given in equation (14) and $\pi(m_2|.m_{.1})$ needs to be normalized for each m_1 value. With this result, one can find the initial mass distribution and compute the probability $P(m_1 > m_{th})$, equation (18), for m_2 masses.

5.2 Results

Using the approach illustrated in Figs 7 and 8, we show m_1 and m_2 distributions at formation time. Different values of k and of the three parameters related to the t_d distribution (t_{max}, t_{min}, z_{max}) are considered. Changing the latter three parameters can reduce the probability of a BH formation with mass below $2\,M_\odot$, but, as long as this PDF is not negligible for $m < 2\,M_\odot$, the tension between observational data and the minimum BH mass will increase with the number of detected BHs. This figure also shows that the $k = 0.5$ case, which was specially studied by Croker et al. (2021) as a GBH model, is the safest among the shown cases in this figure.

By applying the mass factor correction on the PLPP distribution (17), with the best-fit parameters (16), and using equation (18) with $N = 72$, the probability that no merged BBH was formed with mass smaller than $2\,M_\odot$ is $P \approx 2 \times 10^{-4}$, thus implying a minimum tension of 3.7σ for the reference values. With new detections in the current LVK run (O4), assuming that the PLPP profile with the best parameter values and the t_d distribution will remain the same, the tension is forecast to increase beyond 5σ (250 events).

Instead of m_1, one may consider the m_2 masses, which lead to stronger constraints but depend on an additional PLPP parameter, β_q. In our events selection, Table 1, there are 69 m_2 masses larger than $5\,M_\odot$: these are too massive to be NSs. Using the m_2 distribution, equation (20), we find that the tension becomes 4.0σ for $m_{th} = 2\,M_\odot$. Fixing $k = 3$ but reducing the minimum mass, one finds that the tension disappears (i.e. less than 2σ) if $m_{th} < 0.5\,M_\odot$. These results assume the best-fit PLPP parameters. In the following, we return to focus on the m_1 analysis.

In Fig. 9, we show how the tension changes with the BH minimum mass, considering m_1 data. This figure also considers changes in w, in the context of the DEBH model. The tension decreases for larger w values, which implies lower k values. It is important to point out that the case $k = 0.5$ is safe (Croker et al. 2021): the forecast result implies no tension, as expected, since the modified PLPP profile at formation time, Fig. 8, show no relevant probability for $m_1 < 2\,M_\odot$.

In Fig. 10, we show exclusion plots for the DEBH and GBH models considering parameter variations with respect to the reference values (for the 72 observed m_1 data), fixed PLPP parameters as the best values and $m_þ = 2\,M_\odot$. All the reference value changes here considered are such that the tension decreases. This figure should be compared with Fig. 2. Both figures show qualitatively the same

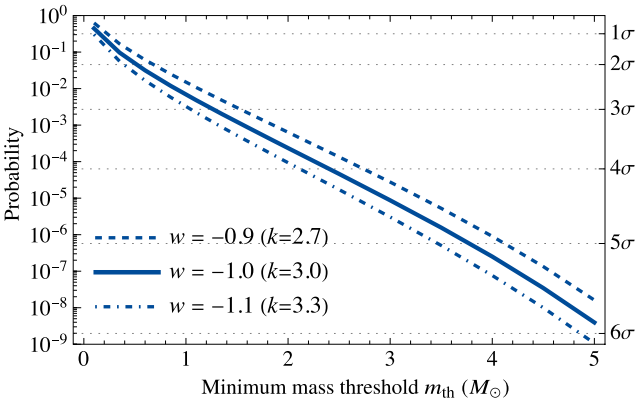

Figure 9. PLPP method. Probability that the DEBH model is in agreement with the minimum BH mass threshold, as a function of the latter, and for different w values. This case uses $k = -3w$.

behaviour, but quantitatively, as expected, the PLPP approach is stronger. We are thus left with only four parameters: k, $t_{\rm min}$, $t_{\rm max}$, and $z_{\rm max}$. We see that, out of these four, the two most important ones which could be changed to alleviate the tension are k (as expected) and $t_{\rm max}$. However, we do not have a physical explanation for using a low $t_{\rm max}$ value (that would require an unexpected restriction on the possible initial conditions of BBHs). For the DEBH model, the tension is reduced by increasing w, which corresponds to decreasing k, but even the case $w = -0.6$, which is far from the standard cosmological model, is not sufficient to drop the tension to an acceptable level. In the following, using Fig. 10, we highlight the necessary individual parameter ranges that reduce the reference tension from 3.7σ to an acceptable level, below 2.0σ. They are: $k \leq 1.7$, $t_{\rm max} < 6$ Gyr, $z_{\rm max} < 2$. Reducing $t_{\rm min}$ from 50 to 5 Myr only marginally improves the picture. Although imposing a strong bound on the maximum delay time value is effective at reducing the tension, there is no clear physical mechanism for this. In principle, BBHs are formed with a large spread on the starting orbit and masses. In the standard picture ($k = 0$), most of them need not to merge within a Hubble time (e.g. Ghodla et al. 2023).

In Fig. 11, we consider how the m_1-based CCBH tension changes by considering 10^3 samples of the PLPP parameter distribution (LIGO Scientific Collaboration, Virgo Collaboration & KAGRA Collaboration 2023) and $m_{\rm p} = 2\,{\rm M}_\odot$. We stress the following properties: *i*) For the $k = 1$ case, the results for the current and forecast data are compatible with no tension (i.e. below 2σ); *ii*) for $k = 3$ case with current data, 95 per cent of the realizations have tension larger than 3.2σ; *iii*) for the forecast with $k = 3$, 95 per cent of the realizations have tension larger than 6σ. *iv*) Although the spread for the PLPP method is larger than for the direct one, the PLPP results are clearly stronger for $k = 3$.

Fig. 12, similarly to Fig. 5, explores the combined variation of the two most relevant parameters for this analysis, k and minimum BH mass ($m_{\rm th}$), and takes into account the full distribution of the PLPP parameters (instead of only using the best-value parameters). The main result is the blue solid line that delimits the 2σ excluded region for the current data. To find this curve, we proceed as follows: for each pair of values (k, $m_{\rm th}$) and a particular realization of the PLPP parameters distribution, we compute the probability that there is no

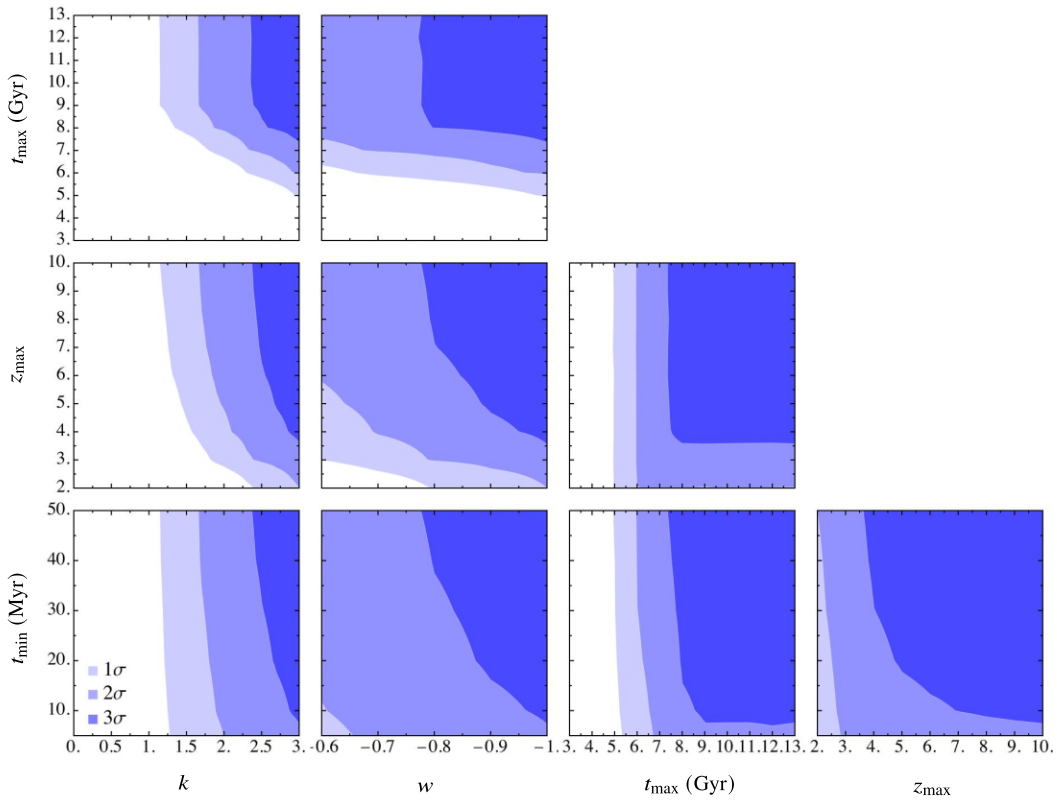

Figure 10. PLPP method. Same as Fig. 2. The GBH and DEBH tensions with observational data, assuming that the PLPP distribution models the detection bias and $m_{\rm th} = 2.0\,{\rm M}_\odot$. The reference values are always in the upper right corner of each plot. The first and second columns correspond, respectively, to the GBH and the DEBH cases. The two last columns show results that are common to both approaches.

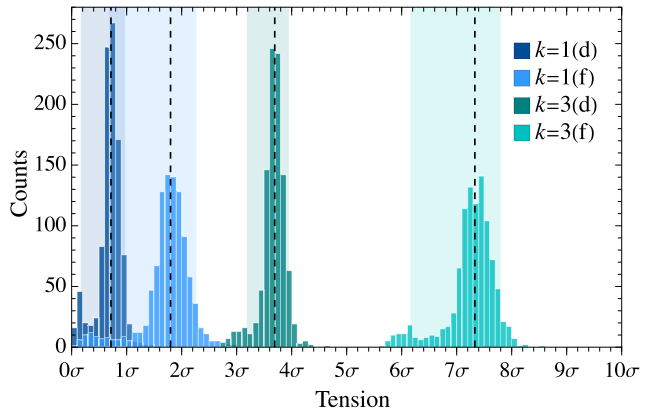

Figure 11. Similar to Fig. 4 for the PLPP method. The histograms show the CCBHs tensions computed from 10^3 different PLPP parameter realizations, including correlations (). The median agrees with the reference values used for the PLPP parameters (16). The rectangular light-coloured regions delimit the 5 and 95 per cent quantiles of the corresponding distributions, thus propagating the uncertainty in the PLPP parameters.

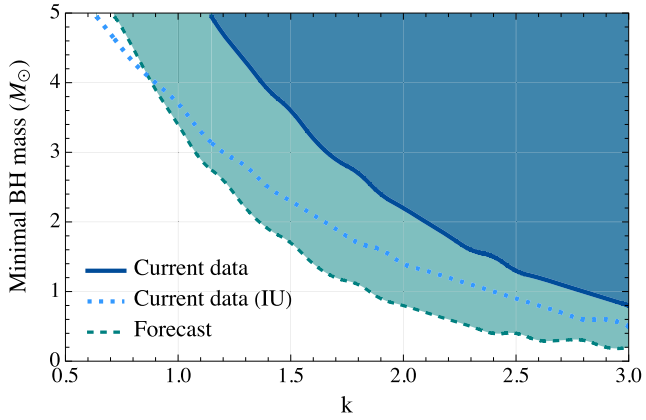

Figure 12. Similar to Fig. 5 for the PLPP method. Excluded regions at 2σ for either the current data (72 events, blueish and solid) or for the forecast (250 events, greenish and dashed), using the GBH approach. The solid and dashed lines consider the full distribution of the PLPP parameters, while the dotted line ignores the uncertainties (IU) and use the best-fit PLPP parameters.

BH with mass below $m_{\rm th}$. We repeat the previous evaluation for 300 realizations of the observational data distribution. A point in the 2σ curve corresponds to the 95 per cent quantile of the previous 300 realizations.

We stress the following results at 2σ level for the current and the forecast data: *i*) assuming $m_{\rm th} = 2\,{\rm M}_\odot$ for the minimum BH mass: $k < 2.1$ (current) and 1.4 (forecast). *ii*) for $k = 3$, $m_{\rm th} < 0.8$ (current) and $0.2\,{\rm M}_\odot$ (forecast). For $k = 1$, there are no constraints from the current data and the forecast yields $m_{\rm th} < 3.4\,{\rm M}_\odot$. For $k = 0.5$, there are no constraints.

6 MODIFIED DELAY-TIME DISTRIBUTION FROM CCBH PHYSICS

In a recent work, Ghodla et al. (2023) (henceforth G23) considered the mass increase of CCBHs in BBHs systems. As discussed in Appendix B, even if individual delay times are significantly different due to the CCBH correction, this does not necessarily imply a change of the $t_{\rm d}$ distribution. Here, we evaluate in detail the consequences within the picture described by G23, showing that this picture indeed leads to changes in the $t_{\rm d}$ distribution, but such changes can only strengthen the constraints we found from the log-uniform case. In the Appendix B, the reason for this behaviour is further explored. G23 find an explicit relation between the delay time of CCBHs with $k > 0$, denoted as $t_{\rm d}$, and an auxiliary delay time that corresponds to the case without cosmological coupling ($k = 0$), here denoted by $\tilde{t}_{\rm d}$. As pointed out by Croker & Weiner (2019); Croker et al. (2021), there are two factors that are important for the BBH dynamics and that are not part of the standard BH picture ($k = 0$), namely: *i*) the emission of GWs becomes stronger with time, since the system is increasing its mass and, *ii*) conservation of orbital angular momentum. For a given BBH with a given initial orbit at formation, these two factors make $t_{\rm d}$ smaller than the corresponding $\tilde{t}_{\rm d}$. The point *i* above is quite clear and intuitive (since more massive binary systems should emit more GWs), the second point is not as obvious as it may seem, and we briefly review this subject.

The issue with angular momentum conservation can be traced to the question: as a CCBH increases its mass proportionally to a^k, should its velocity continue the same as if it had no cosmological mass increase? Unless further details in the microphysics are specified, one cannot present a definitive answer, because it depends on how a CCBH acquires mass and how it interacts with the rest of the Universe. This is beyond the possible cosmological-fluid description of CCBHs since it is about the property of a single BH. The DEBH and GBH pictures need further input to fix this issue. Although imposing momentum conservation can sound like the simplest choice, this, together with the mass increase, leads to preferred-frame effects. Locally, the mass increase violates the particle 4-momentum conservation [$p^\mu p_\mu = -m^2(t)$]; and if 3-momentum (or spatial angular-momentum) is imposed to be conserved while p^μ is not conserved, there is a break of boost invariance, since only p_0 will not be conserved. This is not a problem in itself: since CCBHs are interacting with the Universe, their preferred frame could be the CMB frame, for instance, but this is an additional ingredient to be specified (see also, Avelino 2023, for a related discussion on prefered frames). Moreover, the case with momentum conservation is the one with the strongest phenomenological bounds (see G23). Henceforth, we only consider the case without angular momentum conservation. If the latter is imposed, constraints can only become stronger for any given k.

G23 finds that, for a BBH system without eccentricity, the evolution of the orbit radius r about the centre of mass follows the same corresponding equation as for standard BHs, apart from a correcting factor (with $c = 1$),

$$\frac{{\rm d}r}{{\rm d}t} = -\frac{64}{5}\frac{G^3\mu M^2}{r^3}\left(\frac{a}{a_i}\right)^{3k}, \tag{21}$$

where $M = m_1 + m_2$ and $\mu = m_1 m_2/(m_1 + m_2)$. Terms that depend on a derivatives are negligible. By solving the differential equation above for $r(t)$ and using $r(t_{\rm m}) = 0$ and $t_{\rm m} = t_{\rm d} + t_i$, where $t_{\rm m}$ is the merger time and t_i the initial or formation time, one finds

$$\int_{t_i}^{t_{\rm d}+t_i}\left(\frac{a(t)}{a_i}\right)^{3k}{\rm d}t = \tilde{t}_{\rm d}. \tag{22}$$

This is the relation between the delay times of CCBH and the delay times of standard BHs (see G23). This relation does not impose momentum conservation, otherwise the exponent $3k$ should be replaced by $15k$. Equation (22) provides the value of $t_{\rm d}$ for given $t_{\rm i}$ (assuming $a(t)$, k and $\tilde{t}_{\rm d}$ are given). Actually, we need $t_{\rm d}$ for given $z_{\rm m}$, because the starting point of our analysis is the observational data,

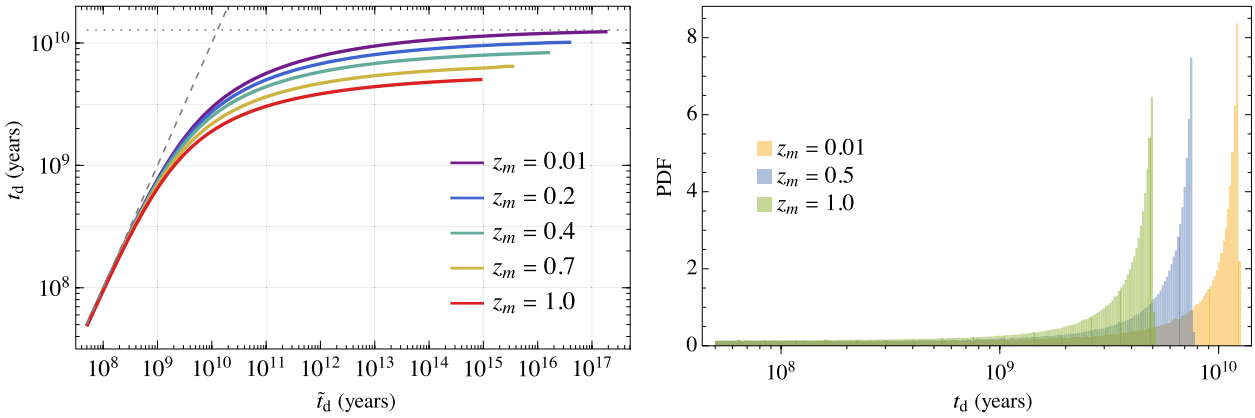

Figure 13. Left. The relation between the physical delay time t_d within the CCBH picture, with $k = 3$, and an auxiliary one, $\tilde{t}_d$, for $k = 0$, at different merger redshifts z_m (see equation (23)). The curves stop at their maximum possible t_d value, such that all BBHs are formed at $z < 10$. The horizontal dotted line is the maximum t_d value for $z_m = 0.01$. The dashed straight line satisfies $t_d = \tilde{t}_d$. Right. Using the log-uniform distribution for $\tilde{t}_d$, the t_d distribution is found as shown in this plot for different z_m values. The modification in the delay time distribution, equation (23), strongly favours larger t_d values.

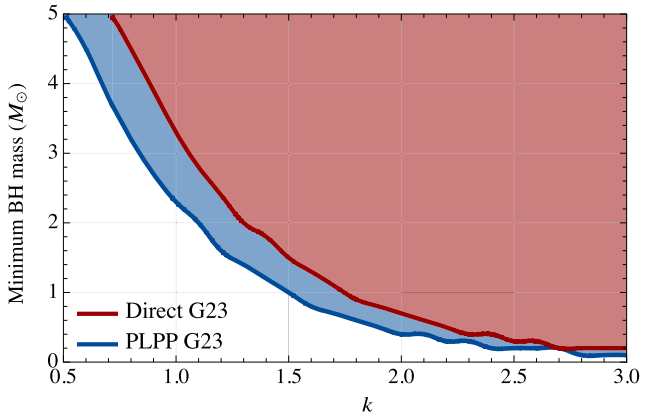

Figure 14. Similar to Figs 5 and 12, but with t_d adjusted for CCBH and only considering current data. Excluded regions at 2σ using either the direct (red) or the PLPP (blue) method. Both curves consider the uncertainties, either in the observational data (direct) or in the PLPP parameters (PLPP).

not the initial configuration. Hence we simply write,

$$\int_{t_m - t_d}^{t_m} \left(\frac{a(t)}{a_i}\right)^{3k} \mathrm{d}t = \tilde{t}_d. \tag{23}$$

Using our reference values for t_d, equation (4), it is possible to plot the relation above for different values of the merging redshift z_m. This is displayed in the left-hand panel of Fig. 13. As can be seen in this panel in the small t_d region, a given $\tilde{t}_d$ interval is mapped into a t_d interval with approximately the same length. However, for large t_d values, a wide interval in the $\tilde{t}_d$ axis corresponds to a much narrower interval in the t_d one. This means that the probability of large t_d values is increased with respect to the $\tilde{t}_d$ distribution. The t_d distribution for different z_m values is shown in detail in the right plot of the same figure.

Fig. 14 combines the direct and PLPP 2σ bounds on the k and the minimum BH mass constraints, it should be compared with Figs 5 and 12. These bounds consider the uncertainties in the observational data and on the PLPP parameters. The constraints are much stronger using the G23 relation. We stress here the same particular cases that were considered before: *i*) assuming $m_{th} = 2\,M_\odot$ for the minimum BH mass: $k < 1.3$ (direct), $k < 1.1$ (PLPP). *ii*) for $k = 3$, $m_{th} < 0.2\,M_\odot$ (direct), $m_{th} < 0.1\,M_\odot$ (PLPP). For $k = 1$, $m_{th} < 3.3\,M_\odot$ (direct), $m_{th} < 2.3\,M_\odot$ (PLPP). For $k = 0.5$, there are no constraints.

7 CONCLUSIONS

According to a recent proposal (Croker & Weiner 2019; Farrah et al. 2023b), BHs grow in mass due to a 'cosmological coupling' and might be responsible for the cosmic acceleration. In such a scenario, dubbed cosmologically coupled BHs, or CCBH, BHs are not of the Kerr type, and are supposed to match asymptotically the cosmological background. This bold idea seems supported by recent analyses of the growth of supermassive BHs in quiescent elliptical galaxies (Farrah et al. 2023a).

In this paper, we tested this hypothesis by considering the binary BHs with stellar progenitors observed with gravitational waves by the LIGO-Virgo-KAGRA (LVK) detectors. If these BHs are cosmologically coupled, they should have undergone a fast mass growth correlated with the cosmological scale factor from the moment of their formation until merging, and should have formed therefore with a mass smaller than the merger one. Since according to the current understanding, there is a mass limit below which stellar BHs cannot form, the presently observed masses could be in conflict with this mass threshold. To compute this conflict, one needs to know the time between the BBH formation and its merger, which is the delay time (t_d). The standard t_d distribution, without cosmological coupling, is the log-uniform one (Abbott et al. 2021a, 2023a). It is not established what the CCBH impact on the t_d distribution would be, since it depends on unknown microphysical details (it may preserve the log-uniform or not). Our main analysis here is based on either the log-uniform distribution or the CCBH-corrected approach of Ghodla et al. (2023). The latter increases our constraints since it favours larger delay times, thus increasing the gap between the formation and the merged mass. This seems to be a general feature of CCBH-corrections to the standard t_d distribution, as discussed in Appendix B. At last, we also study the consequences of a general power-law t_d distribution (Appendix C).

We developed two methods of analysis, one is directly based on the observed events only (direct method), and the other is based on the merged BBH population distribution taking into account observational bias, which uses the power-law-plus-peak distribution (PLPP method). The PLPP distribution is the standard model for the

merged population of BBHs. Once the uncertainties of each method are taken into account, the results are not far from each other. The PLPP approach yields the strongest constraints.

The main result is that the combination of a minimum BH mass with the GWs data from binary compact objects can put strong bounds on the CCBH approach with current data. For $k = 3$ and minimum BH mass ($m_{\rm th}$) of $2\,M_\odot$, a tension of 3σ or more is found with the current data. Moreover, we show that such bounds can quickly be confirmed with new data from LVK and that CCBH corrections to the delay-time distribution commonly enhance the constraints. Specifically, with the current m_1 data for $m_{\rm th} = 2\,M_\odot$: $k < 2.5(1.3)$, for the direct method and $k < 2.1(1.1)$, for the PLPP method at 2σ level. The values in parenthesis use the Ghodla et al. (2023) delay-time correction. Considering the uncertainties on the nature of CCBHs, we also find the required $m_{\rm th}$ value to eliminate the tensions for $k = 3$, and find $m_{\rm th} < 0.5\,M_\odot$. This is a remarkably low value for a BH-like object of stellar origin, as discussed in Appendix A. Finally, for the CCBH variation studied by Croker et al. (2021), whose BH masses increase more slowly ($k = 0.5$), we found no relevant tension with minimum BH masses. This conclusion is also valid for the case $k = 1$, which was recently studied by Cadoni et al. (2023a,b).

At last, we stress that If the LVK BHs are of primordial origin, then a completely different analysis would be needed (see also Ghodla et al. 2023).

ACKNOWLEDGEMENTS

We thank Kevin Croker and Valerio Faraoni for very useful comments and feedback. We also thank Riccardo Sturani for several discussions about this project. LA acknowledges support from DFG project 456622116. DCR thanks Heidelberg University for hospitality and support, he also acknowledges support from *Conselho Nacional de Desenvolvimento Científico e Tecnológico* (CNPq-Brazil) and Fundação de Amparo à Pesquisa e Inovação do Espírito Santo (FAPES-Brazil) (TO 1020/2022, 976/2022, 1081/2022). MQ is supported by the Brazilian research agencies FAPERJ, CNPq (Conselho Nacional de Desenvolvimento Científico e Tecnológico), and CAPES. This study was financed in part by the Coordenação de Aperfeiçoamento de Pessoal de Nível Superior – Brasil (CAPES) – Finance Code 001. We acknowledge support from the CAPES-DAAD bilateral project 'Data Analysis and Model Testing in the Era of Precision Cosmology'.

DATA AVAILABILITY

The data underlying this article are available in the article, in its online supplementary table and in the codes https://github.com/itpamendola/CCBH-direct and https://github.com/davi-rodrigues/CCBH-Numerics.

REFERENCES

Abbott B. P. et al., 2019, Phys. Rev. X, 9, 031040
Abbott R. et al., 2021a, Phys. Rev. D, 104, 022004
Abbott R. et al., 2021b, ApJ, 913, L7
Abbott R. et al., 2022, preprint (arXiv:2212.01477)
Abbott R. et al., 2023a, Phys. Rev. X, 13, 011048
Abbott R. et al., 2023b, Phys. Rev. X, 13, 041039
Abbott R. et al., 2024, Phys. Rev. D, 109, 022001
Akcay S., Matzner R. A., 2011, Class. Quant. Grav., 28, 085012
Andrae R., El-Badry K., 2023, A&A, 673, L10
Avelino P. P., 2023, J. Cosmol. Astropart. Phys., 2023, 005
Belczynski K., Holz D. E., Bulik T., O'Shaughnessy R., 2016, Nature, 534, 512
Cadoni M., Murgia R., Pitzalis M., Sanna A. P., 2023a, preprint (arXiv:2309.16444)
Cadoni M., Sanna A. P., Pitzalis M., Banerjee B., Murgia R., Hazra N., Branchesi M., 2023b, J. Cosmol. Astropart. Phys., 2023, 007
Cardoso V., Pani P., 2019, Living Rev. Rel., 22, 4
Chen Z., Lu Y., Zhao Y., 2022, ApJ, 940, 17
Croker K. S., Weiner J. L., 2019, ApJ, 882, 19
Croker K., Nishimura K., Farrah D., 2020a, ApJ, 889, 115
Croker K. S., Runburg J., Farrah D., 2020b, ApJ, 900, 57
Croker K. S., Zevin M. J., Farrah D., Nishimura K. A., Tarle G., 2021, ApJ, 921, L22
de Sá L. M., Bernardo A., Bachega R. R. A., Horvath J. E., Rocha L. S., Moraes P. H. R. S., 2022, ApJ, 941, 130
Dymnikova I., Galaktionov E., 2016, Class. Quant. Grav., 33, 145010
Faraoni V., Jacques A., 2007, Phys. Rev. D, 76, 063510
Farrah D. et al., 2023a, ApJ, 943, 133
Farrah D. et al., 2023b, ApJ, 944, L31
Fishbach M., Kalogera V., 2021, ApJ, 914, L30
Gao S.-J., Li X.-D., 2023, preprint (arXiv:2307.10708)
Ghodla S., Easther R., Briel M. M., Eldridge J. J., 2023, Open J. Astrophys., 6, 25
Legred I., Chatziioannou K., Essick R., Han S., Landry P., 2021, Phys. Rev. D, 104, 063003
Lei L. et al., 2024, Sci. China-Phys. Mech. Astron., 67, 229811
LIGO Scientific Collaboration, Virgo Collaboration, KAGRA Collaboration, 2023, GWTC-3: Compact Binary Coalescences Observed by LIGO and Virgo During the Second Part of the Third Observing Run – Parameter estimation data release. Zenodo, available at: https://zenodo.org/records/8177023
Mapelli M., 2020, Front. Astron. Space Sci., 7, 38
Mazur P. O., Mottola E., 2015, Class. Quant. Grav., 32, 215024
Mazur P. O., Mottola E., 2023, Universe, 9, 88
Mistele T., 2023, Res. Notes AAS, 7, 101
Morras G. et al., 2023, Phys. Dark Univ., 42, 101285
Özel F., Psaltis D., Narayan R., McClintock J. E., 2010, ApJ, 725, 1918
Parnovsky S. L., 2023, preprint (arXiv:2302.13333)
Rocha L. S., Bachega R. R. A., Horvath J. E., Moraes P. H. R. S., 2021, preprint (arXiv:2107.08822)
Rodriguez C. L., 2023, ApJ, 947, L12
Romani R. W., Filippenko A. V., Silverman J. M., Cenko S. B., Greiner J., Rau A., Elliott J., Pletsch H. J., 2012, ApJ, 760, L36
Talbot C., Thrane E., 2018, ApJ, 856, 173
van Son L. A. C. et al., 2022, ApJ, 931, 17
Wang Y., Wang Z., 2023, preprint (arXiv:2304.01059)
Wolfe N. E., Vitale S., Talbot C., 2023, J. Cosmol. Astropart. Phys., 2023, 039
Ye C., Fishbach M., 2022, ApJ, 937, 73

SUPPORTING INFORMATION

Supplementary data are available at *MNRAS* online.

dataGWevents.csv

Please note: Oxford University Press is not responsible for the content or functionality of any supporting materials supplied by the authors. Any queries (other than missing material) should be directed to the corresponding author for the article.

APPENDIX A: CCBH AND MINIMUM MASS

Here, we discuss the adopted $2\,M_\odot$ as the main value for the minimum BH mass in the CCBH context. We also add considerations about possible future confirmations of low mass BHs.

Neutron star (NS) stability studies based on the Tolman–Oppenheimer–Volkoff (TOV) equation predict that non-rotating NS could have masses at least as high as $2.2\,M_\odot$ (Legred et al. 2021; Ye & Fishbach 2022), which sets a lower bound for Kerr BHs forming through stellar collapse (this bound need not be satisfied for general horizonless compact objects). Incidentally, rotating NS have been measured with masses as high as $2.7\,M_\odot$ (Romani et al. 2012), and studies of binary systems containing NS find an empirical upper limit as high as $2.6\,M_\odot$ (Rocha et al. 2021). This constraint of $2.2\,M_\odot$ was used in the main results of Rodriguez (2023) and Andrae & El-Badry (2023).

Since GBHs simply grow proportionally to a^k, they may or may not have a horizon. On the other hand, DEBHs (which are a type of GEODE, Croker & Weiner 2019) need be a source of DE, thus such objects are not expected to have a horizon. They could be named non-singular BHs or exotic compact objects (ECOs; Mazur & Mottola 2015; Cardoso & Pani 2019). The limit of $2.2\,M_\odot$ need not to apply to them (e.g. Croker & Weiner 2019; Rodriguez 2023; Farrah et al. 2023b).

Although non-singular BHs may form from the stellar evolution (e.g. Mazur & Mottola 2015, 2023) and they may avoid the above horizon-based mass bound, they need to be compatible with the observed NSs with masses as high as $\sim 2.5\,M_\odot$, as above mentioned. BH-like objects with masses about one solar mass are not commonly expected to be of stellar origin. For instance, Abbott et al. (2022) study the possible detection of such objects with LVK, but they are considered to be either of primordial cosmological origin (PBHs) or arising from the collapse of dark matter (which is possible for some particular dark matter models). In the literature on BHs and NSs, there is a large discussion on the mass gap that separates the maximum non-rotating NSs masses from the minimum detected BH ones. At least currently, there is no support for the generation of stellar BHs with about one solar mass or below. Considering the current scenario, $2\,M_\odot$ is a conservative minimum BH mass (i.e. lower than other standard limits), even in the DEBH scenario, considering the lack of a microphysical theory to generate such low-mass BHs from stellar evolution.[4] None the less, we also do several specific tests with other minimum mass values.

We consider now the consequences of a low mass BH detection. If observed BHs are assumed to be a primordial one, then our analysis would not apply, since the t_d distribution should be considerably different. We only consider BHs of stellar origin. Morras et al. (2023) present moderate significance evidence for a subsolar compact object detection of mass $m_2 = 0.76^{+0.50}_{-0.14}\,M_\odot$ at $z_m = 0.028$ (it is the low mass companion of the binary system). This is not a strong evidence, since there are still 16 per cent of chance of its mass being above $1\,M_\odot$, and hence that it could be a NS. None the less, the consequences of a confirmation would be remarkable. Possibly this can be achieved with either the next LVK run or the next generation of GW detectors, as the Einstein Telescope (e.g. Wolfe, Vitale & Talbot 2023). If such a small mass compact object exists and is indeed a BH-like object of stellar origin, it is possible to infer an upper bound on the minimum BH mass value using our methods. Here, we only consider the direct method, since we are only adding a new event and we are not assuming that we know the population of merging low mass BHs.

For comparison, we consider two sets of m_2 data. The first set is composed by all the 72 m_2 events listed in Table 1, apart from the two least massive ones, which are assumed to be NSs by LVK. For this set, the least massive BH has a mass of $2.6\,M_\odot$. The second set is composed by the previous data plus the Morras et al. (2023) object, with mass $0.76\,M_\odot$.

[4]Gao & Li (2023) consider $k > 0$ to explain the mass gap.

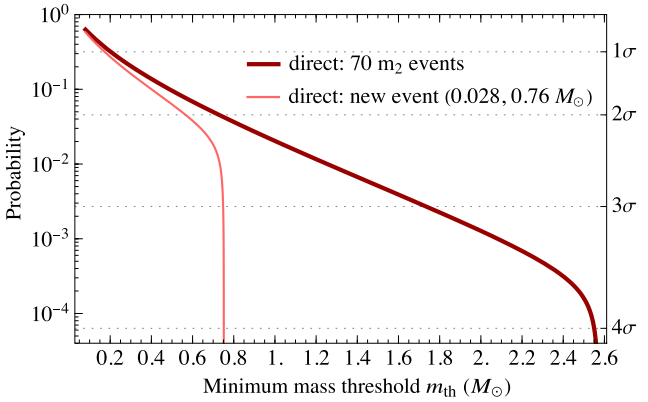

Figure A1. Same as Fig. 3 but using m_2 data and only for $k = 3$. We use two different data sets: one with 70 m_2 events from Table 1, including the event with $m_2 = 2.6\,M_\odot$ and a second data set that adds the Morras et al. (2023) object as a stellar BH with $m_2 = 0.76\,M_\odot$ and $z_\mathrm{m} = 0.028$.

For the first data set and for $k = 3$, the minimum BH mass threshold should satisfy $m_\mathrm{th} < 0.73\,M_\odot$ at 2σ level. Once the Morras et al. (2023) object is considered, one finds $m_\mathrm{th} < 0.57\,M_\odot$. Fig. A1 shows further details. In this figure, as the threshold becomes closer to the detected BH mass, the probability quickly goes to zero.

The above application shows that, as expected, the less massive the detected BH, the smaller should be the minimal CCBH mass to avoid tension with the observational data. To compute a rejection level for given k, one needs a reasonable theoretical estimate for a minimum stellar BH mass. For the particular case considered above, if such estimate is below $0.57\,M_\odot$, there would be no tension with the current data for $k = 3$ (neglecting detection bias).

The delay time distribution has a central role for the constraints we find. The next two appendices are devoted to the t_d distribution.

APPENDIX B: CCBH-MODIFIED DELAY-TIME DISTRIBUTIONS COMPARED WITH THE LOG-UNIFORM ONE: GENERAL APPROACH

Here, we consider the impact of CCBH on the delay-time distribution under general considerations that only depend on certain basic qualitative expectations. We show that the CCBH correction to the delay time distribution is not expected to decrease the chances of finding larger t_d values with respect to the log-uniform distribution. It is shown that the particular correction that preserves the log-uniform distribution is a power-law correction, while exponential corrections and polynomials will increase the likelihood of high t_d values. In Section 6, the particular realization studied by Ghodla et al. (2023) is considered.

Considering CCBHs as true for some fixed k value ($0 < k \leq 3$), and for a given BBH configuration with given initial masses and initial orbit, one can in principle compute both the expected physical delay time t_d within this CCBH framework and an auxiliary delay time $\tilde{t}_\mathrm{d}$ that ignores the cosmological coupling effects ($k = 0$). These delay times are expected to satisfy $t_\mathrm{d} < \tilde{t}_\mathrm{d}$ since the cosmological coupling increases the BHs masses (thus it reduces the time needed from BBH formation up to the merger). More precisely, we will consider the following hypotheses that naturally emerge from this setting: *i*) there exists a function T that maps physical delay times into auxiliary ones, and this function has an inverse: $\tilde{t}_\mathrm{d} = T(t_\mathrm{d})$ and

$t_{\rm d} = T^{-1}(\tilde{t}_{\rm d})$. Since the physical delay time is always smaller than the corresponding auxiliary one, $t_{\rm d} < T(t_{\rm d})$. *ii*) Since the CCBH effects are expected to become larger as the delay-time increases, $T(t)$ needs to increase faster than linearly. *iii*) The minimum and maximum limits of the physical delay-time $t_{\rm d}$ are assumed to be known from physical considerations (e.g. considering the maximum redshift at which BBHs can be formed, simulations on the minimum physical time that stellar-formed BBHs need to merge, etc...). They are denoted by $t_{\rm min}$ and $t_{\rm max}$, respectively. *iv*) The auxiliary delay time is expected to describe the physics with $k = 0$, thus its distribution is assumed to be log-uniform and given by the PDF

$$\tilde{\pi}(\tilde{t}_{\rm d}) = \frac{1}{\ln(\tilde{t}_{\rm max}/\tilde{t}_{\rm min})}\frac{1}{\tilde{t}_{\rm d}}, \tag{B1}$$

where $\tilde{t}_{\rm max} \equiv T(t_{\rm max})$ and $\tilde{t}_{\rm min} \equiv T(t_{\rm min})$ are the maximum and minimum values of the log-uniform distribution. Since $\tilde{t}_{\rm d}$ is simply an auxiliary quantity, computed assuming that $k = 0$, $\tilde{t}_{\rm max}$ can be larger than the age of the Universe.

The four considerations above are more general than the specific assumptions of Ghodla et al. (2023) and they are sufficiently precise to yield that $\log t_{\rm d}$ is not flatly distributed, apart from a specific case, and in general the $\log t_{\rm d}$ is crescent. Indeed, since there is a continuous one-to-one map between $t_{\rm d}$ and $\tilde{t}_{\rm d}$, the probability of finding a physical $t_{\rm d}$ between the values $t_{\rm min}$ and t can be found from $\tilde{\pi}$,

$$P(t) = \int_{t_{\rm min}}^{t} \pi(t_{\rm d})\,{\rm d}t_{\rm d} = \int_{\tilde{t}_{\rm min}}^{\tilde{t}} \tilde{\pi}(\tilde{t}_{\rm d})\,{\rm d}\tilde{t}_{\rm d}, \tag{B2}$$

where $\pi(t_{\rm d})$ is the *a priori* unknown PDF of $t_{\rm d}$ and $\tilde{t} = T(t)$. Therefore, using equation (B1), followed by a redefinition of units,

$$P(t) = \frac{1}{\ln(\tilde{t}_{\rm max}/\tilde{t}_{\rm min})}\ln\left(\frac{T(t)}{\tilde{t}_{\rm min}}\right) = \frac{\ln T(t)}{\ln \tilde{t}_{\rm max}}. \tag{B3}$$

About the units redefinition, one can measure $t_{\rm max}$ and t in units of $t_{\rm min}$, which is in practice equivalent to $t_{\rm min} = 1$. Moreover, since equation (B3) is invariant under $T(t) \to kT(t)$ and $\tilde{t}_{\rm min} = T(1)$, one can set $\tilde{t}_{\rm min} = 1$ in this equation. These units transformations are not necessary, but may be helpful to understand the essence of the argument.

Now we compare the above probability to a log-uniform probability defined within $1 = t_{\rm min} < t < {\rm max}$ and denoted by $\bar{P}(t)$,

$$\frac{P(t)}{\bar{P}(t)} = \frac{\ln t_{\rm max}}{\ln \tilde{t}_{\rm max}}\frac{\ln T(t)}{\ln t}. \tag{B4}$$

If $\ln T(t)$ increases faster than $\ln t$ for all t, then $P(t)/\bar{P}(t)$ monotonically increases, implying that $\max[P(t)/\bar{P}(t)] = P(t_{\rm max})/\bar{P}(t_{\rm max}) = 1$. That is, $P(t) < \bar{P}(t)$ for any $t < t_{\rm max}$. This implies that the $t_{\rm d}$ distribution will not be log-uniform and that it will favour larger $t_{\rm d}$ values with respect to the log-uniform case.

A special $T(t)$ function that is in agreement with $\partial_t[T(t)/t] > 0$ (as implied by the item *ii* above) but $\partial_t[\ln T(t)/\ln t] = 0$ is $T(t) = t^n$, with $n > 1$ and $1 < t < t_{\rm max}$. For this case, although $T(t)$ increases faster than t, $\ln T(t)$ increases proportionally to $\ln t$, implying a constant $P/\bar{P}$ ratio. Indeed, computing equation (B4) directly, $\ln \tilde{t}_{\rm max} = n \ln t_{\rm max}$ and $\ln T(t) = n \ln t$, hence $P(t)/\bar{P}(t) = 1$. A CCBH correction that can be approximated by $T(t) = t^n$ will not change the log-uniform distribution. Exponentials and polynomials, for example, when used to build monotonically increasing $T(t)$ functions, will change the delay-time distribution and will increase the odds of large delay times with respect to the log-uniform case.

We remark that $T(t)$ functions that satisfy the item *ii* (i.e. $\partial_t[T(t)/t] > 0$), cannot lead to $\partial_t[\ln T(t)/\ln t] < 0$.

Provided that the four (*i*–*iv*) general hypothesis listed above are satisfied, and that a log-uniform distribution is a good approximation for the standard ($k = 0$) case, we conclude that the CCBH correction to the standard delay time should either preserve the log-uniform distribution and our results from the Sections 4 and 5, or strength the constraints we find.

APPENDIX C: CHANGING THE DELAY TIME DISTRIBUTION SLOPE

The delay time distribution is a crucial assumption, so we discuss here briefly the impact of changing the $1/t_{\rm d}$ slope. This case is different from the one studied in Appendix B, since here we do not consider CCBH corrections to the log-uniform distribution, but a direct change in the $t_{\rm d}$ distribution.

The full functional form of the relation delay times versus mass is unknown, and it appears difficult to model exactly. Here we limit ourselves to a preliminary investigation. For this appendix, we adopt the more conservative direct method of Section 4. van Son et al. (2022) show a tendency for low-mass BHs to be formed via the common envelope channel, and this channel would have a delay time distribution steeper than $1/t_{\rm d}$ (i.e. shorter delay times on average), corresponding to $\beta = 1.1$–1.3. Looking at the results of appendix B of van Son et al. (2022), we see that such a steeper power-law distribution approximates the predicted behaviour for masses below $30\,{\rm M}_{\odot}$. For simplicity, we assume that this power law extends to all masses; this has anyway very little impact since large masses are not the main drivers of our statistics. In Fig. C1, we show the probability contour plot for w, β. Negative β seems totally excluded. For $\beta \geq 1.2$, the probability for $w = -1$ decreases below 2σ, bringing the DEBH model into the non-rejection region. Therefore, as far as current data are concerned, such steeper power laws might alleviate or solve the tension.

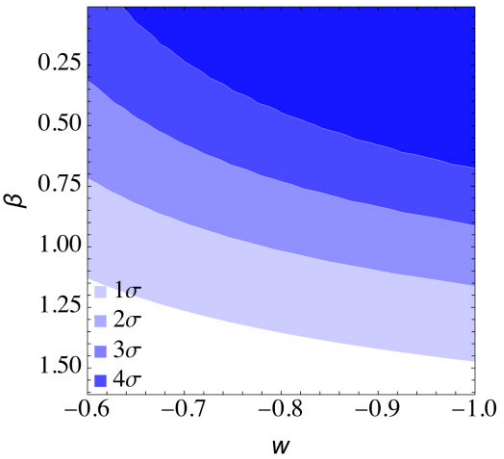

Figure C1. Direct method. Contour plot of $P(m_1 > m_{\rm th})$ as a function of w and the slope β in the DEBH model.

This paper has been typeset from a TEX/LATEX file prepared by the author.